Comparison Between Laser-Induced Nucleation of ZnS and CdS Nanocrystals Directly Into Polymer Matrices

Athanassia Athanassiou,[1,2] Laura Blasi,[1] Milena De Giorgi,[1] Gianvito Caputo,[1] Despina Fragouli,[1] Elsa Tsiranidou,[3] Anna Maria Laera,[4] Leander Tapfer,[4] Roberto Cingolani[1,2]

[1]*NNL-National Nanotechnology Laboratory, INFM, CNR, Via Arnesano, 73100 Lecce, Italy*

[2]*IIT-Italian Institute of Technology, Via Morego 30, Genova, Italy*

[3]*Institute of Electronic Structure and Laser (IESL), FORTH, 711 10 Heraklion, Crete, Greece*

[4]*ENEA, Centro Ricerche Brindisi, SS7 Appia Km 706, I-72100 Brindisi, Italy*

The nucleation of two kinds of crystalline nanoparticles, zinc sulfide (ZnS), and cadmium sulfide (CdS), is achieved directly into specific sites of polymer matrices after their irradiation with UV laser pulses. The starting samples consist of polymers doped with precursors of Zn or Cd thiolate that are proved to decompose after the absorption of UV light, resulting into the nanoparticles formation. The growth of the crystalline nanostructures is followed throughout the irradiation of the samples with successive incident pulses, by different methods, such as transmission electron microscopy, atomic force microscopy, confocal microscopy, and X-ray diffraction. Special attention is paid to the difference of the formation pathways of the two kinds of nanoparticles studied, because the Cd thiolate precursor exhibits much higher absorption efficiency than the Zn thiolate one, at the applied UV wavelength. Indeed, CdS nanoparticles become evident after the very first incident UV pulses, whereas the formation of ZnS nanocrystals requires rather prolonged irradiation, always through a macroscopically nondestructive procedure for the polymer matrix. POLYM. COMPOS., 31:1075–1083, 2010. © 2009 Society of Plastics Engineers

INTRODUCTION

The research activity on the combination of semiconductor nanocrystals with polymeric materials has grown rapidly recently [1–6], aiming to the enhancement of diverse properties of the polymers, such as optical, mechanical, electronic, and magnetic. The polymers that are used as matrices are usually inexpensive and easily manufactured, processed and manipulated, properties that make the resulting nanocomposite materials ideal for a number of applications, such as optical filtering, solar cells, light-emitting diodes, photodetectors, and gas sensors [1–9]. Furthermore, the aggregation of the nanoparticles, a commonly encountered problem in the colloidal nanocrystal synthesis, can be prevented by the appropriate incorporation techniques of the particles into the polymer matrices, giving homogeneous nanocomposite samples with enhanced properties [4, 5, 10, 11]. For this reason, systematic research goes on for the appropriate combination and mixing of nanocrystals with polymeric matrices [12]. An advantage of the nanocomposite samples involved in applications dealing with absorption or emission of light is that their optical properties can be tuned by changing the size of the incorporated nanocrystalline semiconductors in the range of the Bohr exciton radius of the nanocrystals. This range is extended typically from few to few tens of nanometers, and the optical tuning effect is due to the variation of the semiconductor band gap with the size of the nanocrystals, when this gets smaller than the Bohr exciton radius [13–15]. In particular, the smaller the nanocrystal, the larger its effective band gap, and eventually, the greater the energy of optical emission resulting from electron–hole recombination.

In the present work, we report on *in situ* nanocomposite formation by the nucleation of metal sulfide nanoparticles directly into the polymer matrix, starting from the matrix incorporating the metal thiolate precursors of the nanoparticles. The decomposition of metal thiolate precursors through thermal annealing to produce metal and metal sulfide nanoparticles had been previous reported for ZnS [16], CdS [17], HgS [18], Cu_2S [19], and Au [20].

Correspondence to: A. Athanassiou; e-mail: athanassia.athanassiou@unile.it
DOI 10.1002/pc.20894
Published online in Wiley InterScience (www.interscience.wiley.com).

Either spherical nanocrystals or nanorods were produced initiating from the same precursors by changing the annealing temperature and time [19]. The nucleation and growth of metal sulfide nanoparticles directly into a polymer matrix have also been reported in the literature by heating of the polymeric samples with the thiolate precursors at temperatures between 230 and 300°C [21–24].

In a recent work, we demonstrated, for the first time, the possibility of using pulsed laser irradiation for the formation of metal sulfide nanocrystals, and specifically CdS, in the quantum size regime [25], directly into well-confined areas of a polymer matrix, starting from the polymer incorporating cadmium-bis-dodecanthiolate precursor, without inducing any macroscopic damage to the host matrix. Additionally, it was studied how the specific precursor is affected by different irradiation conditions, such as the wavelength [26]. Irradiation at a wavelength where the precursor is bad absorber causes the reduction of the formation speed of the CdS nanocrystals [26]. In the present work, we confirm the possibly to generalize the applicability of this method for the preparation of nanocomposite samples with localized properties, by investigating two kinds of precursors that absorb differently at a specific applied laser wavelength. In particular, we examine the *in situ* formation of metal sulfide nanocrystals after irradiation with laser light at wavelength 308 nm of the thermoplastic cyclo-olefin copolymer Topas doped with the precursors zinc bis-dodecanthiolate and cadmium bis-dodecanthiolate, respectively. The former precursor shows low absorption, whereas the latter exhibits a clear absorption peak close to the applied wavelength. Transmission electron microscopy (TEM), atomic force microscopy (AFM), X-ray diffraction (XRD), and confocal microscopy are used to reveal the mechanisms of the gradual nucleation of the two kinds of nanocrystals into the polymer matrix.

EXPERIMENTAL

Preparation of Polymer/Precursors Composite Films

For the fabrication of the polymer nanocomposites, zinc thiolate $Zn(SR)_2$, $R = C_{12}H_{25}$ and cadmium thiolate $Cd(SR)_2$, $R = C_{12}H_{25}$ precursors were synthesized and added to the polymer Topas. Topas is a thermoplastic cyclo-olefin copolymer consisting of ethylene and norbonene chains, transparent in the visible. The chemical reaction formula for the preparation of the precursors, which is described in detail in Refs. 22 and 23, is

$$M(NO_3)_2 \cdot 6H_2O \xrightarrow[\substack{(i)NH_4OH_{(aq)} \\ (ii)2C_{12}H_{25}SH}]{EtOH} M(SC_{12}H_{25})_2 \quad (1)$$

where M is zinc (Zn) or cadmium (Cd). Twenty percent by weight of metal thiolate was mixed with 80% by weight of Topas, and then diluted in toluene. The solutions were sonicated for 30 min to obtain the maximum dispersion of the insoluble cadmium/zinc-bis(thiolate). The solutions were finally casted in petri capsules where, after evaporation of toluene, the films were formed. The geometrical structure of the precursors dispersed in the matrix is discussed analytically elsewhere [22, 24].

Irradiation of the Polymer/Precursors Composite Samples

For the formation of the nanocrystals in the polymer matrices, the samples were irradiated with increasing number of pulses using a XeCl excimer laser (wavelength $\lambda = 308$ nm, pulse duration $t_p = 30$ ns, fluence $F = 100$ mJ·cm^{-2}, and repetition rate 2 Hz). The laser beam was focused perpendicularly onto the surface of the samples to an area of 0.2×0.4 cm^2. Irradiation was performed under air atmosphere. The laser fluence and the repetition rate were low enough to prevent any macroscopic changes on the surface of the polymers, but efficient enough for the formation of nanocrystals. After irradiation, the samples were checked under optical microscope to make sure that the surface remained macroscopically intact. The only noticeable change was in the color of the irradiated area, which became light yellow. This color change was not observed in the Topas samples without the metal-bis (thiolate) precursors, even after a very large number of incident pulses.

Characterization of the Samples

Absorption measurements were performed with a UV-visible-NIR scanning spectrophotometer, Cary-5000 Varian, on samples of few hundreds of nanometers thickness, prepared on quartz substrates.

The micro/nanoscale topographic features of the nanocomposite films were investigated with an atomic force microscope SMENA-B (NT-MDT) working in semi-contact mode in air (at 20°C, relative humidity 30%) using MPP-12120 silicon probes (Veeco) with a resonant frequency of about 150 kHz. In some cases, topographic and phase images were recorded simultaneously.

The XRD measurements were performed by employing an X-ray diffractometer using CuKα radiation (Rigaku, Dmax 2400, 12 kW, Cu Target, Bragg-Brentano geometry). The XRD measurements were used for crystal structure identification of the formed nanoparticles and for determination of their size. All the samples were measured with the diffractometer in coupled $\theta/2\theta$ sample-detector scans. The measurements were performed before and after irradiation of the polymer/precursors films to verify the phase changes of the precursor to the nanocrystals.

Spatially resolved photoluminescence measurements have been performed on the irradiated samples by means of a confocal system (Olympus FV1000) in epilayer configuration with a spatial resolution of 500 nm. The sam-

 DOI 10.1002/pc

ples were excited by an UV diode laser ($\lambda = 405$ nm) through an objective lens (magnification 40×) with a numerical aperture of NA = 0.80.

Low-magnification TEM images of the laser-synthesized nanocrystals were recorded with a Jeol Jem 1011 microscope operating at an accelerating voltage of 100 kV. The samples for TEM analyses were prepared by dropping a dilute solution of the irradiated part of the sample dissolved in chloroform, onto carbon-coated copper grids and then allowing the solvent to evaporate. Next, the grids were immediately transferred to the TEM microscope and analyzed.

RESULTS AND DISCUSSION

An initial study on the absorption spectra of the as-prepared samples of the Topas polymer incorporating the thiolate precursors showed a significant difference in the absorption characteristics between the two samples under investigation. As demonstrated in the absorption spectra presented in Fig. 1, the UV wavelength used for the irradiation experiments (308 nm) is weakly absorbed by the samples containing the Zn-thiolate precursor, because they exhibit absorption peaks at wavelengths smaller than 250 nm. Conversely, the samples containing the Cd-thiolate precursor have an absorption peak at longer wavelengths, with a tail that clearly is extended beyond the applied wavelength. The absorption spectra of the undoped polymeric matrix of Topas polymer is also shown for comparison reasons.

Next, the polymer/precursors films were irradiated with successive laser pulses at 308 nm to investigate the possible formation of nanocrystals in the irradiated areas. For this purpose, the samples after their irradiation were examined by XRD. As presented in Fig. 2, crystalline structures are present in both kinds of samples. However, in the case of the Cd-thiolate precursors, the peaks of the crystalline structures start being evident after a much smaller number of incident pulses than in the case of the Zn-thiolate precursors (Fig. 2a and b). Because of the high background noise of the XRD spectra, apparent crystalline peaks were monitored for the Cd-thiolate films after 20 pulses and for the Zn-thiolate films after 150 pulses. Evidence for such peaks already appear in lower number of pulses but the signal is obscured by the noise. The Bragg diffraction peaks that are formed in the case of the Cd-thiolate precursors are attributed to the hexagonal phase of CdS (crystal symmetry $P6_3mc$ and lattice constants a = 4.121 Å and c = 6.682 Å). In the case of the Zn-thiolate precursors, all the diffraction peaks can be indexed to the hexagonal phase of ZnS (h-ZnS) with wurtzite structure, with the lattice constants of a = b = 3.819 Å, c = 6.257 Å. The angular positions and relative peak intensity heights coincide with the values reported in the Joint Committee on Powder Diffraction Standards-International Center for Diffraction Data (JCPDS-ICDD), Powder Diffraction File (PDF): 80-0006.

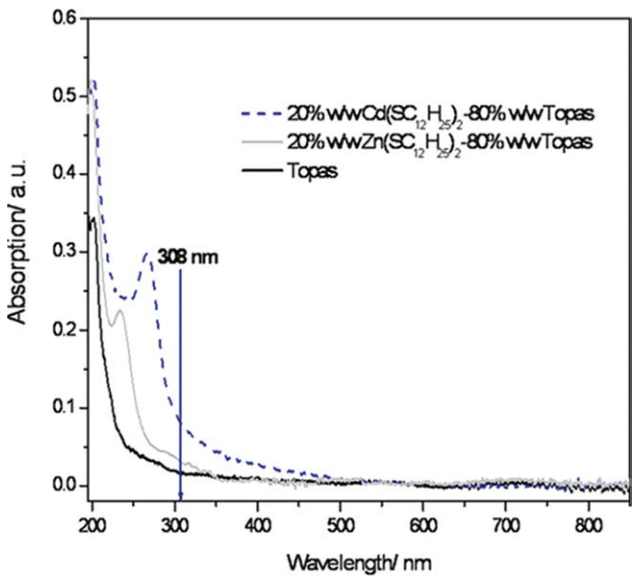

FIG. 1. Absorption spectra of the Topas polymer and of the Topas containing Cd-thiolate and Zn-thiolate precursors. [Color figure can be viewed in the online issue, which is available at www.interscience.wiley.com.]

Each of the measured Bragg diffraction peaks at the angles corresponding to the CdS and ZnS structures was fit with a Gaussian function whose full width at half maximum (FWHM) is related to the diameter of the formed nanocrystals (D). The relationship is given by the Debye–Scherrer formula for spherical particles, shown in *Eq. 2* [27, 28].

$$D = \frac{\lambda}{\Delta\omega_{2\theta} \cdot \cos\theta_B} \tag{2}$$

where λ is the wavelength of the X-ray used ($\lambda_{CuK\alpha} = 0.154$ nm), $\Delta\omega_{2\theta}$ is the FWHM of the Bragg diffraction bands, and θ_B is the Bragg angle of diffraction.

Following the Debye–Scherrer formula, the mean diameter of the formed ZnS nanocrystals was found to be 35.0 nm for the samples irradiated with 180 laser pulses, and very similar, about 40.0 nm for the samples irradiated with 300 laser pulses, which is much larger than the exciton Bohr radius of ZnS (2.4 nm) [29, 30]. The estimation of the size of the formed nanoparticles at a smaller number of incident pulses would be very approximate because of high background noise. Because of the same reason, the diameter of the formed CdS crystals could be safely calculated only in the samples irradiated with more than 50 pulses, and their mean size was found around 40.0 nm. For this number of irradiation pulses, the average size of the formed nanocrystals is quite larger than the size of an exciton in the macrocrystalline CdS material (7–8 nm) [10, 31–35].

From the XRD patterns, we could also obtain quantitative information on the increase of the density of the produced nanocrystals on increasing number of pulses. From

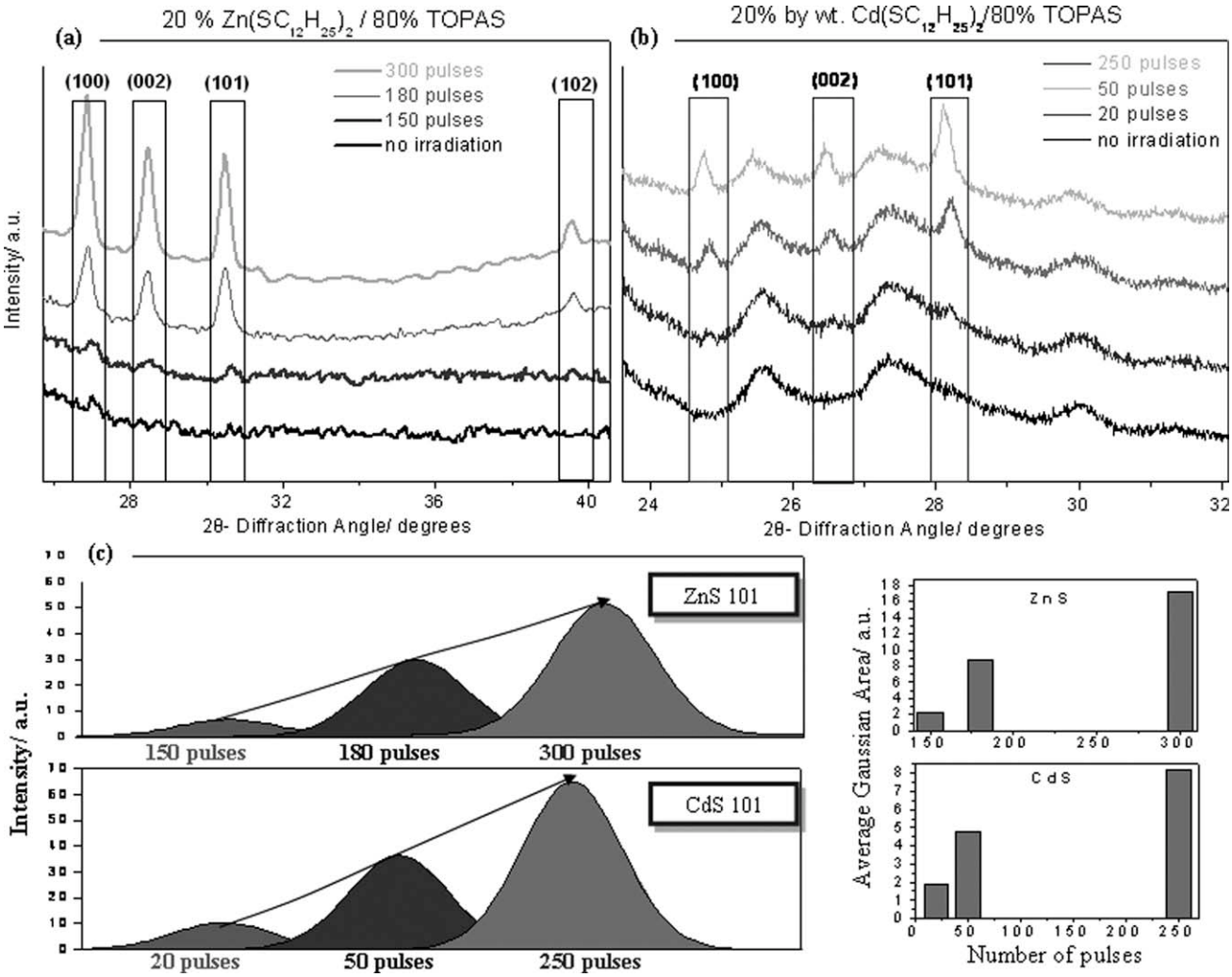

FIG. 2. XRD patterns before and after laser irradiation of the samples of Topas containing the (a) Zn-thiolate precursor and (b) Cd-thiolate precursor. The number of laser pulses used is shown in figure. (c) Comparative display of the Gaussian fits of the crystalline peak (101) formed after irradiation with 20, 50, and 250 pulses successively for the CdS nanoparticles, and after irradiation with 150, 180, and 300 pulses successively for the ZnS nanoparticle. In the two insets are presented the average areas under the Gaussian fits of all the XRD bands versus the number of pulses, for ZnS and CdS nanocrystals.

Fig. 2a and b, it is clear that the intensity of the formed crystalline peaks, which is connected with the number of the nanocrystals in the samples, is amplified as the number of incident pulses increases. For a straightforward quantitative evaluation, we present in Fig. 2c, as a characteristic example, the comparison of the Gaussian fits of the crystalline peak (101) formed after irradiation with 20, 50, and 250 pulses successively for the CdS nanoparticles, and after irradiation with 150, 180, and 300 pulses successively for the ZnS nanoparticles. We performed a fit of all the ZnS and CdS bands (100, 002, and 101) in the XRD pattern with the Gaussian function and we compared the areas under the fitted curves, for the different number of incident pulses. The average areas under the Gaussian fits of all the XRD bands versus the number of pulses are demonstrated in the insets of Fig. 2 for both kinds of nanocrystals. From their comparison, we can safely assume that the density of the formed CdS nanocrystals rises $\sim$2.5 times as the number of pulses increases from 20 to 50, whereas it becomes $\sim$4.5 times bigger when the incident pulses arrive at 250. In the case of the ZnS nanocrystals, their density increases by $\sim$4.0 and $\sim$8.0 times when the incident pulses augment from 150 to 180 and 300, respectively. From these findings, it seems that the density of the ZnS nanocrystals rises much faster than this of the CdS, as soon as they start forming.

AFM measurements were performed on the samples before and after irradiation with a specific number of UV laser pulses to monitor any possible indication for nanoparticles formation at their surfaces (Fig. 3). All the samples before irradiation seem quite smooth without any evidence of nanostructures on their surface, as demonstrated in the characteristic images of Fig. 3a and d. In the case of the polymer samples with the Cd-thiolate pre-

 DOI 10.1002/pc

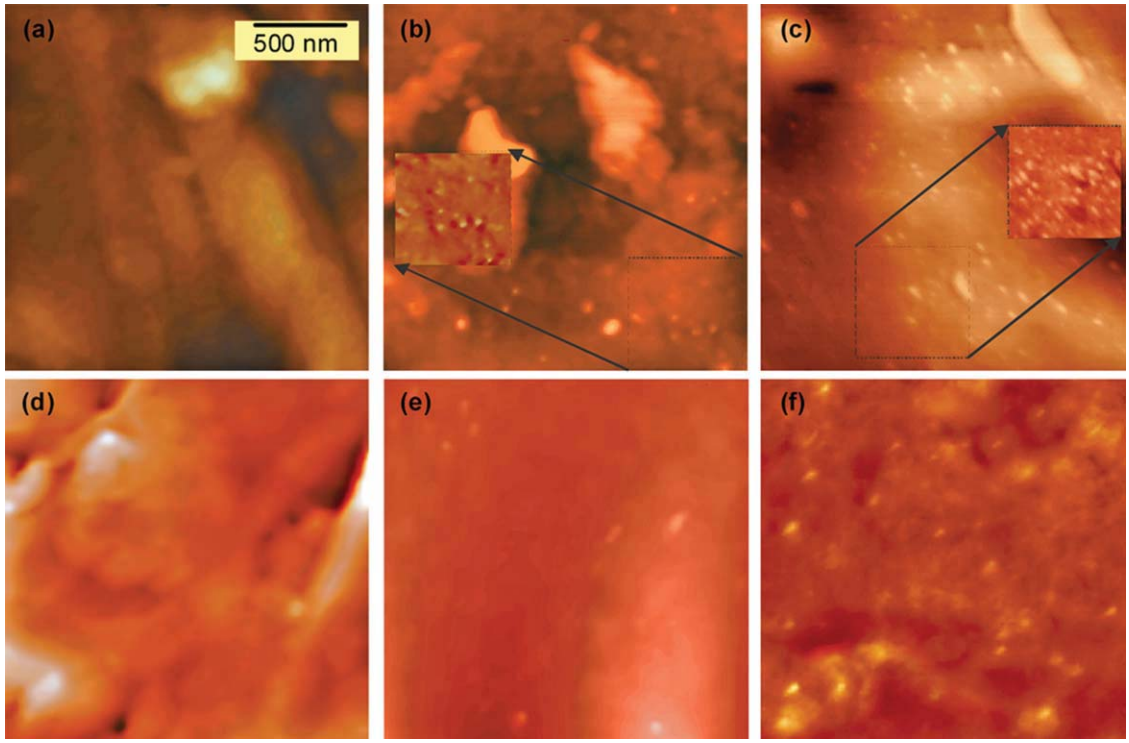

FIG. 3. AFM surface topography images of polymer films containing Cd-thiolate precursors before any irradiation. (a) After irradiation with 10 UV pulses (vertical scale: 0–40 nm) and (b) after irradiation with 50 UV pulses (vertical scale: 0–150 nm) and of (c) polymer films containing Zn-thiolate precursors before any irradiation. (d) After irradiation with 180 UV pulses (vertical scale: 0–130 nm) and (e) after irradiation with 300 UV pulses (vertical scale: 0–160 nm). (f) In the insets of images (b) and (c) are shown phase-contrast images (vertical scale: 55 deg corresponding to image), where the nanoparticles features appear enhanced. The scale bar is the same for all the images and the scanning frequency 1 Hz. [Color figure can be viewed in the online issue, which is available at www.interscience.wiley.com.]

cursor, the AFM images reveal structures of nano-objects floating at the surface already after irradiation with 10 laser pulses, which were not existing before irradiation (Fig. 3b). The image presented in Fig. 3c reveals increased number of nanoparticles at the surface of the samples after 50 laser pulses, indicating that the density of the nanocrystals increases with increasing number of pulses. The phase images, being able to detect variations in the composition of the diverse materials because of the differences in the physical characteristics, provide a clearer evidence of the formation of the nanocrystals on the surface of the polymer matrix (insets 3b and 3c) [36]. Because of the common tip or probe artifact, a phenomenon specific to AFM, that manifests itself in a broadening of the lateral dimensions of surface topography of very small objects, we cannot derive any safe conclusion regarding the dimensions of the formed nano-objects. On the other hand, the vertical resolution of the AFM images is not affected by the finite size of the probe. Therefore, we can safely claim that the height of the formed nanoparticles varies from 2 to maximum 15 nm very close to the exciton size of the CdS (7–8 nm) [10, 31–35]. Parts of the nanocrystals are also expected to be bound in the polymer. For the samples containing the Zn-thiolate precursor, the AFM measurements, in coincidence with the XRD measurements, reveal that a much greater number of laser pulses is needed for the formation of the characteristic structures of the nanocrystals. As shown in Fig. 3e and f, after irradiation with 180 UV laser pulses, only few nanocrystalline structures appear, whereas, after irradiation with 300 UV pulses, the characteristic structures of the nanocrystals are much denser. For samples irradiated with less number of pulses, there was no evidence of the nanoparticles formation on their surfaces.

For an evaluation of the size and distribution of the formed CdS nanocrystals in the irradiated samples containing the Cd-thiolate precursor, fluorescence images were taken with the confocal microscope in the wavelength range 475–540 nm. This is the range where the emission of the CdS nanocrystals is expected to occur, because the bulk semiconductor CdS emits around 512 nm (band gap of 2.42 eV), and for nanocrystals smaller than the Bohr exciton radius of the semiconductor, the emission is shifted towards shorter wavelengths. From the images presented in Fig. 4a and b it is clear that, in the case of the samples irradiated with 50 pulses, the density of the emitting particles is increased compared with that for the samples irradiated with 10 pulses. For samples

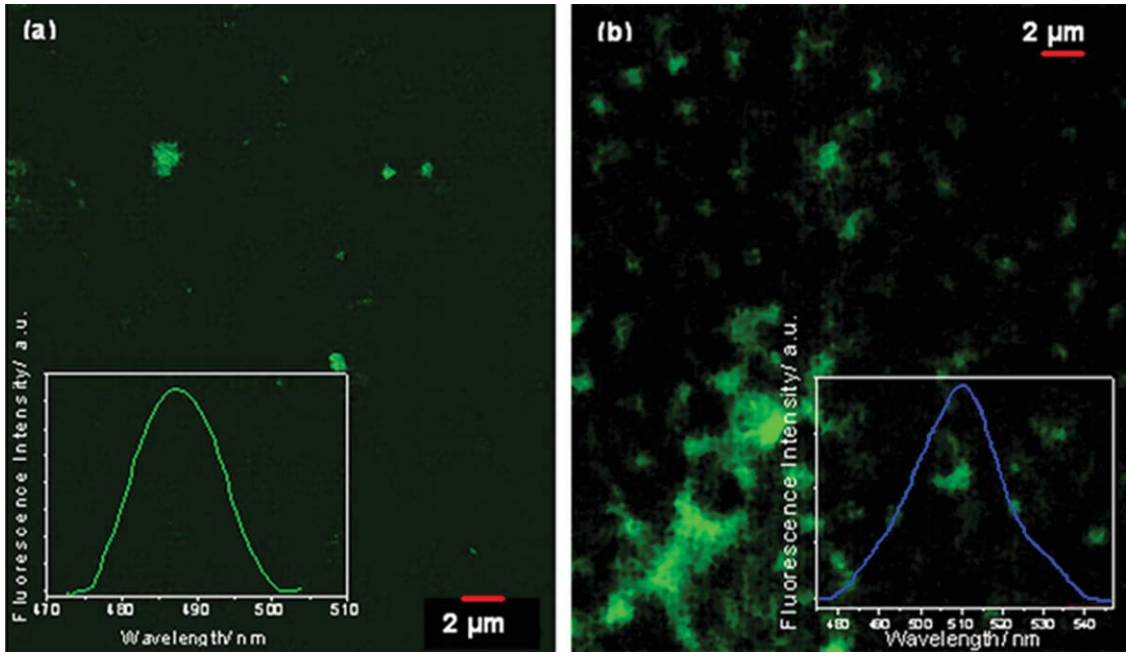

FIG. 4. Fluorescence images taken with the confocal microscope from the samples of Topas containing Cd-thiolate precursor, after irradiation with (a) 10 UV pulses (b) 50 UV pulses. In the insets are shown characteristic emission spectra from each sample. [Color figure can be viewed in the online issue, which is available at www.interscience.wiley.com.]

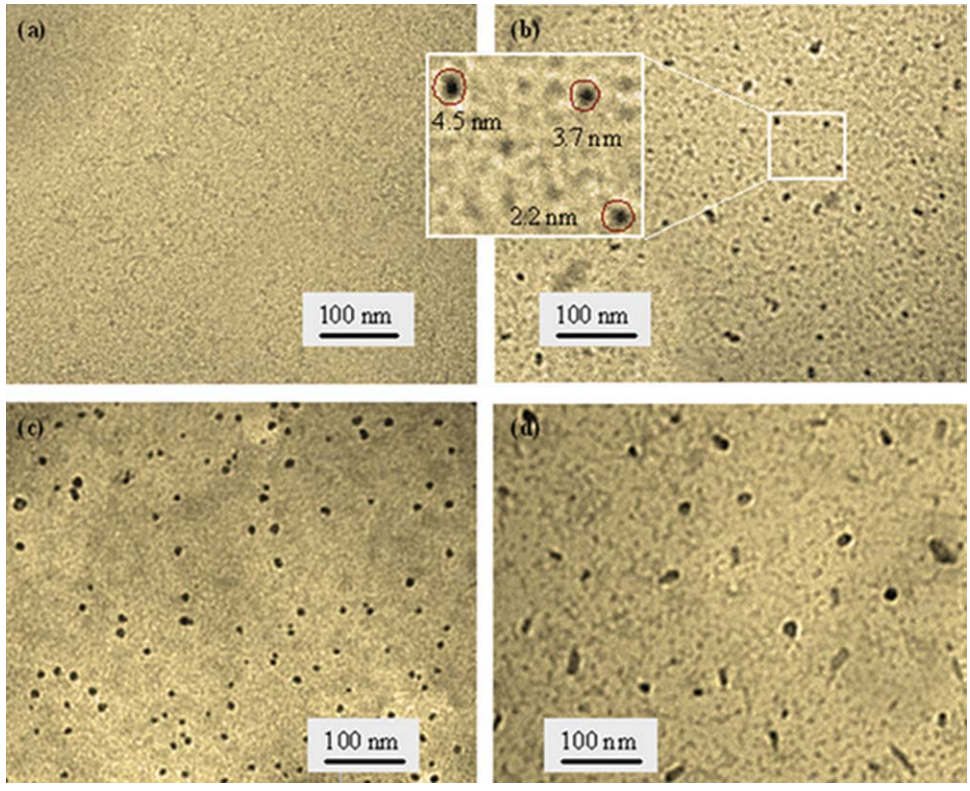

FIG. 5. TEM images of polymer films containing with Zn-thiolate precursors deposited onto a TEM grid. (a) Before any irradiation and (b) after irradiation with 150 UV pulses (inset: magnified nanoparticles). (c) After irradiation with 300 UV pulses. (d) After irradiation with 1000 UV pulses. [Color figure can be viewed in the online issue, which is available at www.interscience.wiley.com.]

 DOI 10.1002/pc

irradiated with five pulses, very few emitting particles could be monitored. The confocal system gives also the possibility to monitor the emission of the single particles through an optical grating and a photomultiplier tube, using as excitation wavelength 405 nm. The typical emission of the nanoparticles formed after 10 UV pulses was found to be in the area between 480 and 500 nm, whereas for the nanocrystals formed after 50 UV pulses it is shifted towards longer wavelengths, with the central one around 510 nm. It should be mentioned here that a shift in the emission wavelength is also monitored in some cases also for nanocrystals created in the same sample, due to the variation in their size. The red shift was monitored exclusively in the emission of samples with increasing number of incident pulses, between a few and 50, revealing that in this range of incident pulses the formed nanoparticles are in the quantum size regime [21]. Above 50 pulses, no further shift of the emission wavelength was monitored, indicating that above this number of pulses nanocrystals with bulk material properties are exclusively formed. The confocal microscope images reveal that there are areas where the nanoparticles are preferentially formed, but due to the limited spatial resolution of the instrument it is impossible to evaluate if in these areas individual nanoparticles are formed or if they are coagulated.

For the ZnS nanocomposite samples, the confocal measurements could not be performed because the excitation wavelength of 405 nm was in the same range of the emission wavelength of these nanocrystals. Therefore, to get an in-depth knowledge for the size and the distribution of this kind of nanoparticles in the matrix, we performed low-magnification TEM analysis. The images of the unirradiated samples showed no indication of nanoparticles. On the other hand, the measurements on the irradiated samples revealed that the formation of the ZnS nanoparticles has already started after the irradiation of the samples with 150 UV pulses, impossible to be monitored with the other experimental methods. The TEM images from the samples irradiated with 150 and 300 pulses, presented in Fig. 5b and c, respectively, show that the size distribution between the two nanocomposite samples is quite similar (a couple to 20 nm), but the density of the formed nanocrystals is bigger in the second case. It should be mentioned here that some of the measured nanoparticles are very close to the ZnS Bohr radius, *i.e.* 2.4 nm, so they are in the quantum size regime [29, 30]. For the samples that are irradiated with 1000 pulses, bigger nanocrystals seem to be formed, mainly with rod-like shapes (10–50 nm long). The formation of the bigger particles or nanorods might be attributed to the coalescence of neighboring particles. The formation of one-dimensional structures starting from small particles that agglomerate to bigger clusters that are coalescing together forming nanorods is also observed for ZnS nanocrystals formed by simple evaporation technique [37]. The size of the formed nanoparticles estimated using the XRD technique seems to be quite bigger compared with the one evaluated from the TEM images. A plausible reason for this differentiation is that in the case of formation of aggregates on the irradiation process, the procedure of the dilution of the irradiated samples for their deposition onto the TEM grid nanoparticles might have an impact on the dimensions of the eventually deposited nanoparticles, because any coagulated particles can be partly dissolved and separated.

Two possible mechanisms can be proposed for the nucleation of the nanocrystals into the polymer matrices after the UV irradiation: the direct photolysis or the indirect thermolysis of the precursors. In any case, the formation of the nanocrystals should be described by the following mechanism

$$\mathrm{M(SC_{12}H_{25})_2/Topas} \overset{\mathrm{hv,heat}}{\rightarrow} \mathrm{MS/Topas + S(C_{12}H_{25})_2}, \quad \mathrm{M: Cd, Zn} \qquad (3)$$

The mechanism of photolysis is expected to be more efficient in the case of the Cd-bis(thiolate) precursor that is a better absorber in the applied wavelength of 308 nm (Fig. 1). Therefore, the CdS nanocrystals are expected to be formed much faster than the ZnS ones, in agreement with all our experimental observations. The absorption of the Cd-bis(thiolate)/Topas is calculated about five times higher than that of the Zn-bis(thiolate)/Topas corrected for the Topas absorption. This value is quite approximate taking into account possible inhomogeneities of the samples. On the other hand, the initiation of the formation of the ZnS nanocrystals starts after a number of UV pulses about 15 times greater than that needed for the formation of CdS. This implies that the photolysis efficiency of the two precursors as well as the efficiency of the formation of the two metal thiolates do not correspond to the absorption efficiency of the respective samples. Indeed, the formation of the ZnS is slower than expected by the absorption measurements presented in Fig. 1. A similar result, although using thermal treatment of the films, was reported by Antolini et al. [24] where on annealing at 290–300°C of the precursors/polymers films, the formation of CdS nanocrystals needs 10 min, whereas the formation of ZnS occurs after 15 min, demonstrating lower formation efficiency of the ZnS.

In the case of the zinc-bis(thiolate) precursor, an extra thermolysis mechanism can also contribute to the formation of ZnS nanocrystals, although the relative contribution of each mechanism cannot be evaluated quantitatively. Indeed, absorption measurements performed on a pure Topas film after irradiation with laser pulses at 308 nm and fluence 100 mJ cm^{-2} revealed that on increasing number of pulses the polymer exhibits increased absorption at 308 nm (Fig. 6). Therefore, photoproducts of the Topas polymer absorbing around 308 nm are formed on extensive UV irradiation. Munzert et al.

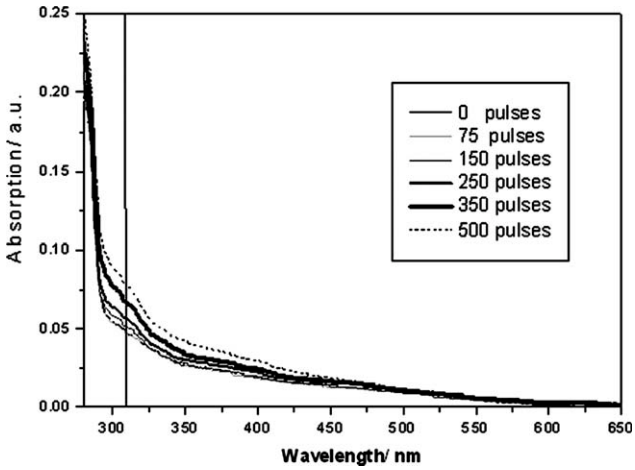

FIG. 6. Absorption spectra of the Topas polymer on irradiation with increasing number of UV pulses.

[38] also showed that on UV irradiation of the Topas matrix are formed photoproducts that absorb in the UV, but their measurements were performed at wavelengths quite higher than 308 nm. Figure 6 reveals that the absorption of the formed photoproducts around 308 nm starts being evident after 150 pulses, which is close to the number of pulses needed for the observation of the ZnS nanocrystals. This number of pulses is too high to affect the formation of the CdS nanocrystals, that reach already the bulk material properties after 50 laser pulses. Therefore, it is plausible that after the absorption of the incident photons from the Topas photoproducts, formed after numerous laser pulses, the resulting thermal energy of their relaxation is deposited on the Zn-thiolate precursor and thermally decompose it, contributing to the formation of the ZnS nanocrystals. The possibility that above a certain number of pulses ($\sim$150) an extra mechanism is contributing to the formation of the ZnS nanocrystals is enhanced by the XRD finding that the density of the ZnS nanocrystals seems to rise faster than this of the CdS for increasing number of pulses, as soon as ZnS starts forming. Nevertheless, also in the case of the ZnS, the formation of the nanocrystals is localized in the areas that the UV light irradiation occurs, and the procedure, although possibly through different mechanisms, is efficient for the nanoparticles formation in both the cases of the precursors.

CONCLUSIONS

It is demonstrated that on pulsed UV irradiation it is feasible to form structures of semiconductor nanocrystals in polymer films, which increase their size and density on increasing number of pulses. Critical role in the formation of the nanocrystals plays the absorption of the polymer and of the precursors at the used wavelength. Indeed, in the case of the strong absorbing precursor of the CdS, the formation of the nanocrystals is efficiently performed through the direct photolysis of the precursors, leading to nanocrystals that exhibit the size quantization effect. On the contrary, in the case of the less-absorbing precursor of the ZnS, the photolysis efficiency is low and, thus, the formation of the nanocrystals occurs only after extensive UV irradiation. To the ZnS formation may also contribute the photoproducts of the polymer that absorb in the applied wavelength, possibly inducing indirect thermolysis of the Zn-thiolate precursors. Nevertheless, as the TEM investigation revealed, also in this case the nucleated nanoparticles can be in the quantum size regime.

REFERENCES

1. D. Qi, M. Fischbein, M. Drndić, and S. Šelmić, *Appl. Phys. Lett.*, **86**, 093103 (2005).
2. K. R. Choudhury, Y. Sahoo, and P. N. Prasad, *Adv. Mat.*, **17**, 2877 (2005).
3. B. Liu, H. Li, C.H. Chew, W. Que, Y.L. Lam, C.H. Kam, L.M. Gan, and G.Q. Xu, *Mater. Lett.*, **51**, 461 (2001).
4. L. Chen, J. Zhu, Q. Li, S. Chen, and Y. Wang, *Eur. Polym. J.*, **43**, 4593 (2007).
5. L. Guo, S. Chen, and L. Chen, *Colloid. Polym. Sci.*, **285**, 1593 (2007).
6. S. Jing, S. Xing, F. Dong, and C. Zhao, *Polym. Compos.*, **29**, 1165 (2008).
7. R.J. Nussbaumer, W.R. Caseri, P. Smith, and T. Tervoort, *Macromol. Mater. Eng.*, **288**, 44 (2003).
8. J.H. Park, J.Y. Kim, B.D. Chin, Y.C. Kim, J.K. Kim, and O.O. Park, *Nanotechnology*, **15**, 1217 (2004).
9. K. Suri, S. Annapoorni, A.K. Sarkar, and R.P. Tandon, *Sens. Actuators. B.*, **81**, 277 (2002).
10. J.H. Warner, A.A.R. Watt, and R.D. Tilley, *Nanotechnology*, **16**, 2381 (2005).
11. C. Sciancalepore, T. Cassano, M.L. Curri, D. Mecerreyes, A. Valentini, A. Agostiano, R. Tommasi, and M. Striccoli, *Nanotechnology*, **19**, 205705 (2008).
12. M.E. Mackay, A. Tuteja, P.M. Duxbury, C.J. Hawker, B.V. Horn, Z. Guan, G. Chen, and R.S. Krishnan, *Science*, **311**, 1740 (2006).
13. A. Henglein, *Chem. Rev.*, **89**, 1861 (1989).
14. Y. Zhang, N. Raman, J.K. Bailey, C.J. Brinker, and R.M. Crooks, *J. Phys. Chem.*, **96**, 9098 (1992).
15. M.L. Curri, A. Agostiano, L. Manna, M.D. Monica, M. Catalano, L. Chiavarone, V. Spagnolo, and M. Lugara, *J. Phys. Chem. B.*, **104**, 8391 (2000).
16. W.S. Rees Jr. and G.J. Krauter, *Mater. Res.*, **11**, 3005 (1996).
17. O.F.Z. Khan and P. O'Brien, *Polyhedron*, **10**, 325 (1991).
18. G. Krauter, B. Neumuller, V.L. Goedken, and W.S. Rees Jr., *Chem. Mater.*, **8**, 360 (1996).
19. T.H. Larsen, M. Sigman, A. Ghezelbash, R.C. Doty, and B.A. Korgel, *J. Am. Chem. Soc.*, **125**, 5638 (2003).
20. M. Nakamoto, M. Yamamoto, and M. Fukusumi, *Chem. Commun.*, 1622 (2002).
21. F. Antolini, M. Pentimalli, T.D. Luccio, R. Terzi, M. Schioppa, M. Re, L. Marenghi, and L. Tapfer, *Mater. Lett.*, **59**, 3181 (2005).

 DOI 10.1002/pc

22. T.D. Luccio, A.M. Laera, L. Tapfer, S. Kempter, R. Kraus, and B. Nickel, *J. Phys. Chem. B.*, **110**, 12603 (2006).
23. F. Antolini, T.D. Luccio, M. Re, and L. Tapfer, *Cryst. Res. Technol.*, **40**, 948 (2005).
24. F. Antolini, T.D. Luccio, A.M. Laera, L. Mirenghi, E. Piscopiello, M. Re, and L. Tapfer, *Phys. Status. Solidi. B.*, **244**, 2768 (2007).
25. A. Athanassiou, R. Cingolani, E. Tsiranidou, C. Fotakis, A.M. Laera, E. Piscopiello, and L. Tapfer, *Appl. Phys. Lett.*, **91**, 153108 (2007).
26. D. Fragouli, A.M. Laera, P.P. Pompa, G. Caputo, V. Resta, M. Allione, L. Tapfer, R. Cingolani, and A. Athanassiou, *Microelectron. Eng.*, **86**, 816 (2009).
27. P. Scherrer, *Göttinger Nachrichten* **2**, 98 (1918).
28. A. Guinier, X-Ray Diffraction in Crystals, Imperfect Crystals, and Amorphous Bodies, W. H. Freeman, San Francisco (1963).
29. W.T. Yao, S.H. Yu, and L. Pan, *Small*, **1**, 320 (2005).
30. T. Trindade, *Chem. Mater.*, **13**, 3843 (2001).
31. L. Brus, *IEEE. J. Quantum Electron.*, **22**, 1909 (1986).
32. V. Ladizhansky, G. Hodes, and S.J. Vega, *Phys. Chem. B.*, **102**, 8505 (1998).
33. A. Pan, H. Yang, R. Liu, R. Yu, B. Zou, and Z. Wang, *JACS*, **127**, 15692 (2005).
34. Y.-C. Chu, C.-C. Wang, and C.-Y. Chen, *Nanotechnology*, **16**, 58 (2005).
35. H. Tong and Y.-J. Zhu, *Nanotechnology*, **17**, 845 (2006).
36. M.O. Finot and M.T. McDermott, *J. Am. Chem. Soc.*, **119**, 8564 (1997).
37. S. Velumani and J.A. Ascencio, *Appl. Phys. A.*, **79**, 153 (2004).
38. P. Munzert, U. Schulz, and N. Kaiser, *Surf. Coat. Technol.*, **1048**, 174 (2003).